Gas phase synthesis of epitaxial layers of nickel-chlorine boracite on chromium-chlorine boracite

Schmid, Hans; Tippmann, Heinz

Journal of Crystal Growth 46 (1979) 723–742

GAS PHASE SYNTHESIS OF EPITAXIAL LAYERS OF NICKEL–CHLORINE BORACITE ON CHROMIUM–CHLORINE BORACITE

Hans SCHMID * and Heinz TIPPMAN
Battelle Geneva Research Centre, CH-1227 Carouge-Geneva, Switzerland

Received 11 January 1979

Layers of Ni–Cl boracite have been epitaxially grown on Cr–Cl boracite at 900°C. At the reaction temperature both substrate and layer had the cubic $\bar{4}3m$ symmetry whereas at room temperature the layer is ferroelectric (symmetry mm2) and the substrate is still cubic. The layers have been produced both by (i) CVT reactions in closed quartz ampoules and by (ii) two variants of a CVD process using either the reactants $BCl_3(g) + H_2O(g)$, or $B_2O_3(l) + H_2O(g)$ for the formation of the intermediate gaseous $(BOCl)_3$ and the B_2O_3 hydrates. The reactant $NiCl_2(g)$ has been obtained by the reaction $Ni(s) + Cl_2(g) = NiCl_2(g)$ at about 1000°C inside the reactor. Layer thicknesses from 1 up to 100 μm have been achieved. The growth rate was of the order of 1 μm/min. The best substrates were found to be those with smooth, as-grown surfaces; these layers were characterized after cool-down by a pattern of ferroelectric 180° domains with the spontaneous polarization oriented perpendicularly to the surface, an average domain size between 1 and 10 μm and by good contrast (at λ = 546 nm) between antiparallel domains placed between crossed polarizers and a retarder. The ferroelectric poling fields were $>10^7$ V m^{-1}.

1. Introduction

1.1. Motivation

Orthorhombic boracites are ferroelectric and are characterized by the symmetry species [1] $\bar{4}3mFmm2$. Hence a jumping of the optical indicatrix of the orthorhombic phase by 90° around the orthorhombic *c*-axis (which is parallel to the spontaneous polarization and to the pseudo-cubic ⟨100⟩ direction) can take place upon 180° reversal of the spontaneous polarization [2–5]. This can be achieved by applying a voltage to the electrodes (e.g. transparent Au on Cr [3]) deposited on the facets of wafers cut parallel to pseudocubic (100). This behaviour is similar to that of $Gd_2(MoO_4)_3$, which is characterized by species $\bar{4}2mFmm2$ [6,7]. The switchable spontaneous birefringence at room temperature is about 10–15 times higher in orthorhombic boracites (Δn: 0.004 to 0.022) [4] than in $Gd_2(MoO_4)_3$ (Δn: 0.0004). This means that at equal switching field strength the switching voltage can in principle be made much smaller in the case of boracites, provided they can be produced in the form of relatively thin layers or wafers. Such sheets would be interesting, because applications like light gates, passive display, page composers, etc. can be envisaged [3,5]. Whereas compositions with relatively small birefringence (e.g. Fe–I boracite with $\Delta n_{25°C} = 0.004$) can be used in the form of self-supporting single crystalline wafers, compositions with higher Δn necessitate the fabrication of epitaxial, substrate-supported layers with a thickness of a few microns if a quarter wave device is desired.

The objective of the work described in this paper was to demonstrate the practical feasibility of making such layers by a chemical process.

1.2. Approach

The fabrication of epitaxial boracite layers seemed possible by modifying one of the two previously known methods of obtaining single crystalline boracite, namely: the hydrothermal or hydrothermal-like

* Present address: Department of Inorganic, Analytical and Applied Chemistry University of Geneva, 30, quai Ernest Ansermet, CH-1211 Geneva 4, Switzerland.

method [8–18], or the chemical vapour transport (CVT) method [19–23].

The gas phase approach was finally chosen, because of easier control of the experimental parameters and because it entails less risk of partial replacement of the halogen by OH than the hydrothermal method. Because of the well-known tendency of increase of the Curie temperature in the series I → Br → Cl → F → OH boracite, the partial incorporation of OH was expected to lead to an undesirable increase of switching field strength of hydrothermal halogen boracites.

Table 1
Potential point groups and crystallographic cuts of substrates appropriate for switchable layers of orthorhombic boracite

Crystal system	Point group	Possible cuts
Cubic	m3m, 432, $\bar{4}$3m, m3, 23	(*hh*0), (100)
Tetragonal	$\bar{4}$	(001)
	$\bar{4}$2m	(001)

2. Choice of the substrate material

2.1. The binary axis condition

If a layer of orthorhombic boracite is to be used for contrast modulation by electric field switching of the orientation of the spontaneous birefringence, that layer has to be single crystalline and in its cubic high temperature phase with one of the cubic (100) planes oriented parallely to the surface of the substrate. For the symmetry species $\bar{4}$3mFmm2 of the layer it is mandatory that the substrate surface possesses a binary axis perpendicularly to itself. If, on the contrary, a substrate with a four-fold symmetry axis is used, two kinds of crystallite, mutually related by a $\pi/2$ rotation would be obtained with equal probability, and the average transmission between crossed polarizers and a retarder would remain identical for

Table 2
Estimated data of enthalpy and entropy of formation of some boracites, $M_3B_7O_{13}X$ (units in kcal mole^{-1} and cal deg^{-1} mole^{-1}, respectively)

M	X					
	Cl		Br		I	
	S°_{298}	ΔH°_{298}	S°_{298}	ΔH°_{298}	S°_{298}	ΔH°_{298}
Mg	71.9	−1494	74.7	−1479	76.2	−1460
(Ti) [a]	78.0		80.3		83.5	
(V) [a]		−1361		−1348		−1334
Cr		−1297		−1285		−1277
Mn	95.2	−1345	97.9	−1333	99.5	−1317
Fe	91.8	−1258	92.9	−1247	94.5	−1232
Co	84.2	−1239	87.5	−1228	88.9	−1212
Ni	81.2	−1237	82.3	−1226	83.8	−1210
Cu	94.1	−1174	87.2	−1167	88.7	−1150
Zn	84.4	−1315	87.9	−1304	90.5	−1290
Cd	92.1	−1258	93.9	−1249	98.1	−1236

[a] Boracite unknown.

Remark: Entropy data obtained by Kelley's "sum method" (see e.g. ref. [38]); the ΔH° data given in the table are based on the assumption that the enthalpy of formation from the components MO(s), B_2O_3(s) and MX_2(s) was approximately zero. The real values are probably 5–6% more negative as can be estimated from a comparison of the method applied to Cd and Ca borates [31] of similar metaloxide/B_2O_3 ratio as occurring in boracite. The data for the entropies and enthalpies of the components were taken from ref. [42], those of VO(s) from ref. [19] and S°_{298} of CrO from ref. [43].

both up and down polarity of the applied field. The same is true for a random orientation of crystallites having $(100)_{cub}$ parallel to an isotropic substrate surface, and equally for a polycrystalline ceramic material with prototypic symmetry $\bar{4}3m$.

2.2. The thermal expansion condition

Because the composition of the boracite layer is cubic at the deposition temperature and remains cubic for several hundred degrees during cooling, it is necessary that the thermal expansion coefficient of the substrate is isotropic in the contact plane. This requirement reduces very much the possibilities of choice of the substrate. As shown on table 1, it can be fulfilled for substrates with one of the five cubic point groups or with one of the tetragonal groups $\bar{4}$ or $\bar{4}2m$.

The orthorhombic groups mmm and 222 and the monoclinic group 2/m necessitate special cuts for achieving isotropy of the expansion coefficient. Therefore they are inconvenient. Consideration of the various limitations suggested therefore that a boracite having cubic $\bar{4}3m$ symmetry at room temperature should be used as substrate.

2.3. Optical and chemical conditions

There exist only a few halogen boracites which are with certainty cubic ($\bar{4}3m$) at room temperature: Cr–Cl, Cr–Br, Cr–I, Co–I and Ni–I. Cr–Cl boracite was chosen for two reasons: (i) greatest chemical stability (see table 2) and (ii) good transmission at wavelengths smaller than about 590 nm [24]; this behaviour matches the maxima of transmission of Ni–Cl boracite centring at about 500 and 580 nm [25].

3. Choice of the layer material

For the choice of the composition of the ferroelectrically active boracite layer the following criteria have to be taken into account:

(i) In order to avoid decomposition of the substrate by the reactive atmosphere, the free energy of formation of the substrate should be more negative than that of the layer (see table 2).

(ii) For reasons of easy control of the synthesis, only the bivalent oxidation state of the metal of the layer boracite should be stable.

(iii) Experience with epitaxy of garnets on garnet shows [26] that (a) the difference in lattice parameters of substrate/layer should be less than about 1% (cf. table 3) and (b) the difference in thermal expansion should be negligible in order to avoid dislocations in the layer and cracking.

(iv) To avoid ferroelastic clamping of the domains and concomitant high coercive field, the orthohombic shear angle of the layer material should be $\leqslant 1$ min of arc or preferably zero [3,5].

Ni–Cl boracite was chosen as the layer material because conditions (i), (ii) and (iii) are well fulfilled. Although criterion (iv) is not fulfilled (the shear angle of Ni–Cl boracite is 2.4 ± 1 min of arc [14]) that latter point has no impact on the chemical problem. The experiments suggest that the first criterion is met.

Table 3
Mean cubic lattice parameter misfit [a] of some orthorhombic boracites with cubic Cr–Cl boracite at room temperature

Boracite, mm2 at 20°C	Misfit with Cr–Cl boracite (%)
Mg–Cl	−0.42
Mn–Cl	1.33
Mn–Br	1.39
Mn–I	1.68
Fe–I	0.93
Ni–Cl	−0.70
Ni–Br	−0.71
Cu–Cl	−0.72
Zn–Br	−0.30
Zn–I	−0.25
Cd–Cl	3.00
Cd–Br	3.1
Cd–I	3.6

[a] Definition of misfit = $[\Delta a_{cub}/a_{cub}(\text{mean})] \times 100$.

4. Experimental

4.1. Synthesis of single crystal substrates from $Cr_3B_7O_{13}Cl$

Step I: In a first stage Cr–Cl boracite has been synthetized by the previously described "three crucible

Table 4
Thermochemical data of some hypothetical transport reactions and equilibria of importance in the gase phase synthesis of Ni–Cl boracite

Reaction No	(Transport)*) reaction equilibrium	$(\Delta H^{o}_{298})^{R*)}$ kcal x mol^{-1}	$(\Delta S^{o}_{298})^{R}$ cal x mol^{-1} x deg^{-1}	$(\Delta G^{o}_{1147})^{R}$ kcal x mol^{-1}	lg Kp_{1147}	Ref.
1	$Ni_3B_7O_{13}Cl(s) + 5\ HCl(g) + H_2O(g) \rightleftarrows 7\ HBO_2(g) + 3\ NiCl_2(g)$	+ 436.2	+ 271.0	+ 125.4	- 23.9	(a)
2	$Ni_3B_7O_{13}Cl(s) + 5\ HCl(g) + 8\ H_2O(g) \rightleftarrows 7\ H_3BO_3(g) + 3\ NiCl_2(g)$	+ 118.7	+ 48.1	+ 63.5	- 12.1	(a)
3	$Ni_3B_7O_{13}Cl(g) + 5\ HCl(g) + H_2O(g) \rightleftarrows \frac{7}{3}\ (HBO_2)_3(g) + 3\ NiCl_2(g)$	+ 107.2	+ 63.8	+ 34.0	- 6.49	(a)
4	$Ni_3B_7O_{13}Cl(g) + 12\ HCl(g) \rightleftarrows \frac{7}{3}\ (BOCl)_3(g) + 3\ NiCl_2(g) + 6H_2O(g)$	+ 214.1	+ 86,5	+ 114,9	- 21.9	(a)
5	$B_2O_3(l) + H_2O(g) \rightleftarrows 2\ HBO_2(g)$	+ 89.1	+ 50.7	+ 30.9	- 5.9 (- 17.4)	(a) (c)
6	$B_2O_3(l) + H_2O(g) \rightleftarrows \frac{2}{3}\ (HBO_2)_3(g)$	- 4.92	- 8.48	+ 4.81	- 0.92	(a)
7	$B_2O_3(l) + 3\ H_2O(g) \rightleftarrows 2\ H_3BO_3(g)$	- 1.65	- 12.98	+ 13.24	- 2.52 (- 5.95)	(a) (c)
8	$B_2O_3(l) + 2\ HCl(g) \rightleftarrows \frac{2}{3}\ (BOCl)_3(g) + H_2O(g)$	+ 25.61	- 2.01	+ 27.92	- 5.32 (- 6.70)	(a) (c)
9	$NiCl_2(s) \rightleftarrows NiCl_2(g)$				- 0.855	(13)
10	$NiO(s) + 2\ HCl(g) \rightleftarrows NiCl_2(g) + H_2O(g)$	+ 30.4	+ 19.8	+ 7.69	- 1.47	(a)
11	$(3NiO).B_2O_3(s) + 6\ HCl(g) \rightleftarrows 2\ HBO_2(g) + 3\ NiCl_2(g) + 2\ H_2O(g)$	+ 187.9	+ 115.9	+ 54.96	- 10.48	(a)
12	$(3NiO).B_2O_3(s) + 6\ HCl(g) \rightleftarrows 2H_3BO_3(g) + 3\ NiCl_2(g)$	+ 97.2	+ 52.2	+ 37.33	- 7.11	(a)
13	$(3NiO).B_2O_3(s) + 6\ HCl(g) \rightleftarrows \frac{2}{3}\ (HBO_2)_3(g) + 3\ NiCl_2(g) + 2H_2O(g)$	+ 93.9	+ 56.7	+ 28.87	- 5.5	(a)
14	$(3NiO).B_2O_3(s) + 8\ HCl(g) \rightleftarrows \frac{2}{3}\ (BOCl)_3(g) + 3\ NiCl_2(g) + H_2O(g)$	+ 297.8	- 72.1	+ 380.5	- 72.5	(a)
15	$B_2O_3(l) + 6\ HCl(g) \rightleftarrows 2\ BCl_3(g) + 3\ H_2O(g)$	+ 65.6	- 12.6	+ 80.1	- 15.26	(a)
16	$(BOCl)_3(g) + 6\ HCl(g) \rightleftarrows 3\ BCl_3(g) + 3\ H_2O(g)$	+ 60.1	- 15.9	+ 78,34	- 14.93	(a)
17	$HBO_2(g) + 3\ HCl(g) \rightleftarrows BCl_3(g) + 2\ H_2O(g)$	- 11.72	- 31.67	+ 24.61	- 4.69	(a)
18	$(HBO_2)_3(g) + 9\ HCl(g) \rightleftarrows 3\ BCl_3(g) + 6\ H_2O(g)$	+ 105.8	- 6.23	+ 112.9	- 21.53	(a)
19	$H_3BO_3(g) + 3\ HCl(g) \rightleftarrows BCl_3(g)\ 3\ H_2O(g)$	+ 33.6	+ 0.17	+ 33.41	- 6.37	(a)
20	$Ni_3B_7O_{13}Cl(s) + 26HCl(g) \rightleftarrows 7\ BCl_3(g) + 3\ NiCl_2(g) + 13\ H_2O(g)$	+ 354.2	+ 49.3	+ 297.65	- 56.7	(a) (b)

Legend : (a) calculated from Table 7 data
(b) schematic balance of CVD/BCl_3 process, however kinetically and thermodynamically improbable
(c) from ref. [21] obtained with first approximation for T = 1163°K

*) Remark : for the transport reactions (i.e. one solid reactant) : positive ΔH^{o}_{298} means transport from $T_2 \rightarrow T_1$ ($T_2 > T_1$)

method" [19] working in closed quartz ampoules. In that method the overall reaction

$$MX_2(s \text{ or } l) + 7\ B_2O_3(l) + 5\ MO(s) \rightarrow 2\ M_3B_7O_{13}X(s)$$

(M = metal, X = halogen), is carried out by placing the three condensed reactants in three different crucibles (see fig. 1) and transporting them to the

Table 5
(a)–(g) Growth conditions of Cr–Cl and Ni–Cl boracite

a) $Cr_3B_7O_{13}Cl$, ampoule-method/direct synthesis ⟹ polycrystalline boracite

B_2O_3(gr)	$CrO \rightleftharpoons Cr_2O_3+Cr$(gr)	$CrCl_2$(gr)	H_3BO_3(gr)	temp.(°C)*	temp. profile Nr.	time(hrs)	yield (gr)
2.8	1.6	1.5	0.1	1038	8	132	2.95

b) $Cr_3B_7O_{13}Cl$, ampoule-method/pure transport ⟹ single crystals

B_2O_3(gr)	$Cr_3B_7O_{13}Cl$(gr)	$CrCl_2$(gr)	H_3BO_3(gr)	temp.(°C)*	temp. profile Nr.	time(hrs)	yield (gr)	crystal size
2.8	1.0	1.5	0.1	1040	8	264	0.95	3.5 mm

c) $Ni_3B_7O_{13}Cl$-layer deposition on $Zn_3B_7O_{13}Cl$ - substrate : ampoule method

B_2O_3(gr)	NiO (gr)	$NiCl_2$(gr)	$NiCl_2.6H_2O$ ad $NiCl_2$ (gr)	temp.(°C)*	temp. profile Nr.	time(hrs)	layer thickness (μm)
2.8	1.5	2.6	0.1	900	1	1	100

d) $Ni_3B_7O_{13}Cl$-layer deposition on $Cr_3B_7O_{13}Cl$; ampoule method

B_2O_3(gr)	NiO (gr)	$NiCl_2$(gr)	H_3BO_3(gr)	temp.(°C)*	temp. profile Nr.	time(hrs)	layer thickness (μm)
2.8	1.5	2.6	0.1	900	1	1	2

e) $Ni_3B_7O_{13}Cl$-pure transport : ampoule method ⟹ single crystals

B_2O_3(gr)	$Ni_3B_7O_{13}Cl$(gr)	$NiCl_2$(gr)	$NiCl_2.6H_2O$	temp.(°C)*	temp. profile Nr.	time(hrs)	single crystals	crystal size
2.8	1.1	2.6	0.1	900	1	60		5 mm

f) $Ni_3B_7O_{13}Cl$-layer deposition on $Cr_3B_7O_{13}Cl$; BCl_3/H_2O-process; (Fig. 3)

	outer tube			inner tube							
Cl_2 (cm^3/mn)	N_2 (cm^3/mn)	BlC_3 (cm^3/mn)	N_2 (cm^3/mn)	N_2 (cm^3/mn)	H_2O (cm^3/mn)	HCl (cm^3/mn)	P_{total} (Torr)	temp. (°C)	time (hrs)	layer thickness (μm)	substrate final
2.5	20	0.7	20	283	7	70	500	900	0.5	< 0.5	80

g) $Ni_3B_7O_{13}Cl$-layer deposition on $Cr_3B_7O_{13}Cl$; B_2O_3(l)/H_2O (g)-process (Fig. 3. inset 2) [experiment TMA59]

2.5	20	-	-	85	2.2	20	500	900	3	2

*) valid for bottom of ampoule

growing nuclei by means of gas phase reactions (cf. table 4). In the particular case of Cr boracites, the oxide CrO is not known but can be replaced by a mixture of $Cr + Cr_2O_3$. A small amount of H_3BO_3 is used to provide the H_2O necessary for the vapour transport. The experimental parameters are given in table 5a.

In the case of Cr boracite this method yields mostly polycrystalline boracite cakes inside the crucible containing B_2O_3, and thick crusts of boracite on the outside wall of the crucible. The outside crusts are typical of Cr boracites only and they give the impression of having "crept" over the edge.

Step II: In a second stage Cr–Cl boracite single crystalline platelets and cubes having (100) facets of 3–4 mm^2 have been obtained by chemical vapour transport using the preformed polycrystalline Cr–Cl boracite, obtained in step I, as source material instead of the mixture $Cr_2O_3 + Cr$. Otherwise the three crucible arrangement has been maintained (for experimental parameters cf. table 5b).

This new CVT version of obtaining good boracite crystals by means of a two step process has also proved successful for growing manganese boracites [4]. In that case the two step process is particularly helpful because during step I the presence of free MnO leads to heavy attack of the quartz (risk of explosion!) and to many nuclei leading to polycrystalline material only, whereas the preformed Mn boracite does in no way attack the quartz and the smaller number of nuclei formed in step II lead to larger crystals.

4.2. Epitaxial growth of $Ni_3B_7O_{13}Cl$

The epitaxial growth of Ni–Cl boracite has been carried out by (i) chemical vapour transport (CVT) in closed quartz ampoules and by means of (ii) chemical vapour deposition (CVD) type reactions using an open flow system.

4.2.1. Chemical vapour transport (CVT)

The three-crucible method described previously [19] has been adapted for the production of layers of

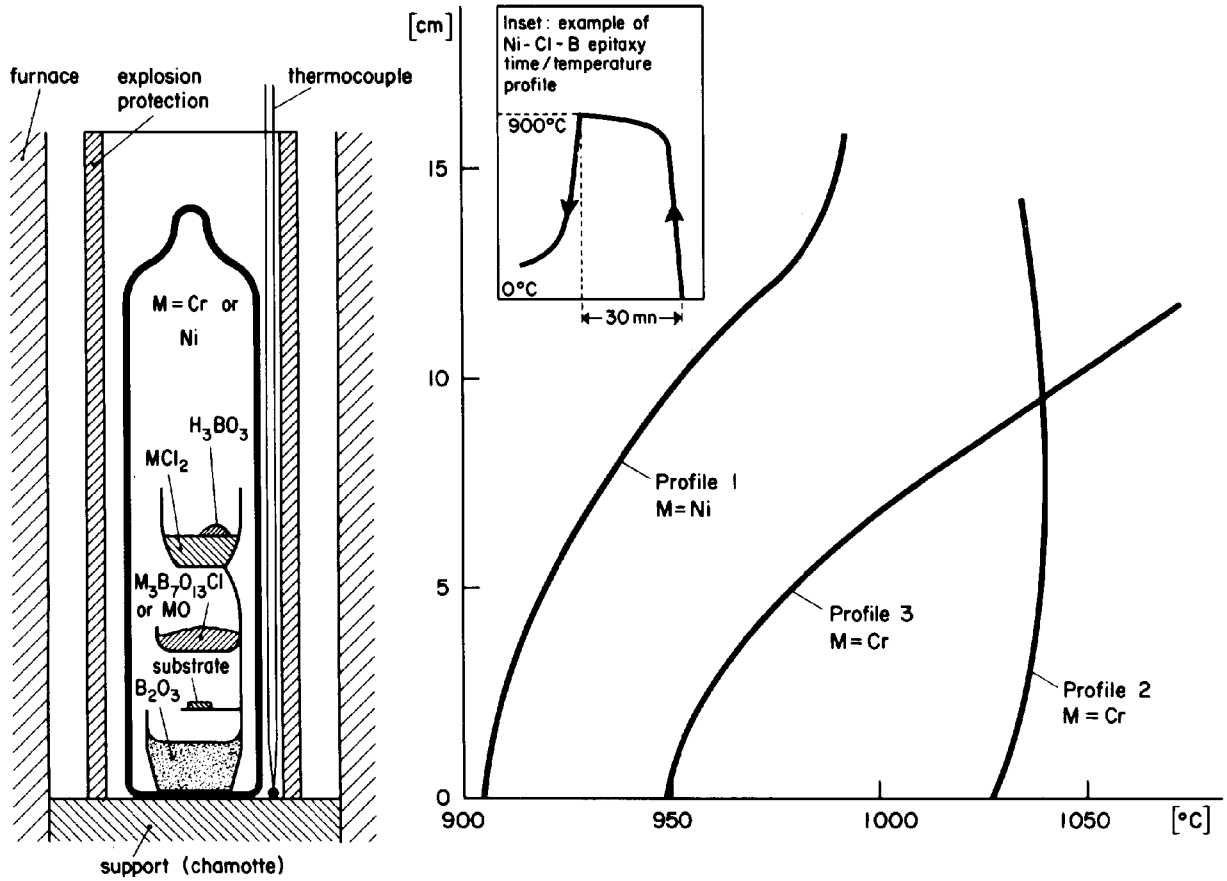

Fig. 1. Transport of boracite in a temperature gradient (three crucible method).

Ni–Cl boracite by placing a quartz substrate holder in between the crucibles containing B_2O_3 and NiO, respectively (cf. fig. 1).

4.2.1.1. Deposition of $Ni_3B_7O_{13}Cl$ on $Zn_3B_7O_{13}Cl$. In a preliminary test run, as-grown Zn–Cl boracite crystals of little value have been used as a substrate. During a one hour run at 900°C a layer of about 100 μm thickness has been obtained (figs. 2a and 2b, table 5c). Zn–Cl boracite is a chemically resistant but not optically acceptable (trigonal at room temperature) substrate for Ni–Cl boracite. The experiment showed, however, the feasibility of the layer production and gave the order of magnitude of the growth rate (about 100 μm/h).

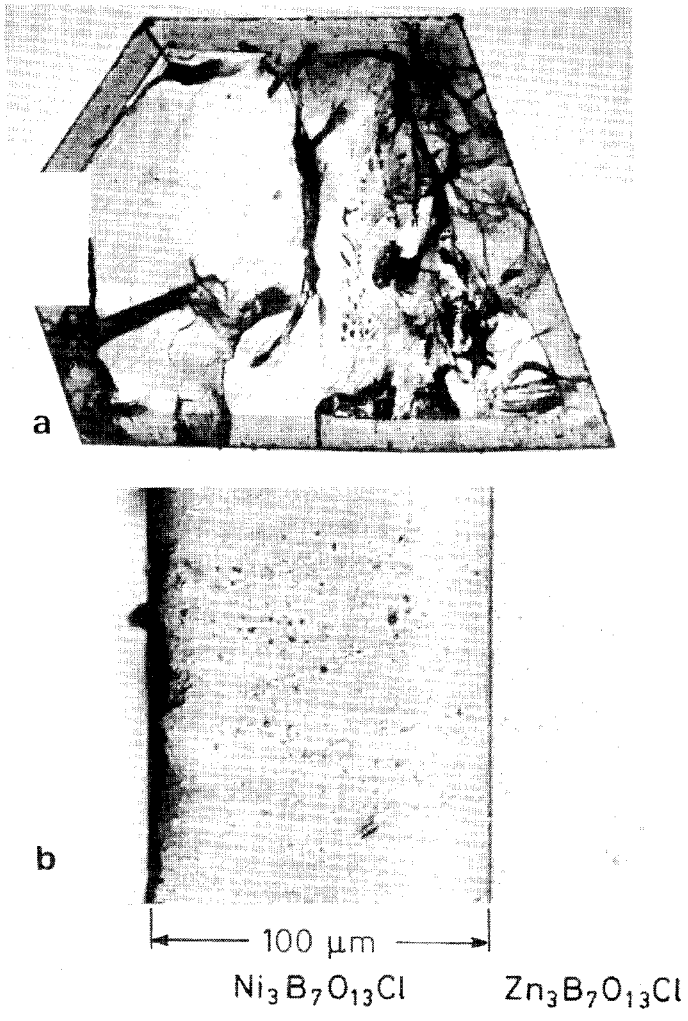

Fig. 2. Transmission photograph of a $(110)_{cub}$-cut Zn–Cl boracite crystal covered with a 100 μm thick layer of Ni–Cl boracite (see section 4.2.1.1); (a) overview, dark zones are fissures in the substrate; (b) detail of (a).

4.2.1.2. Deposition of $Ni_3B_7O_{13}Cl$ on $Cr_3B_7O_{13}Cl$. By using the same experimental arrangement and experimental parameters as described for the deposition on Zn–Cl boracite (section 4.2.1.1), Ni–Cl boracite has been deposited on Cr–Cl boracite (cf. table 5d). The growth rate at 900°C ranged between 40 and 100 μm/h) for the ten experiments carried out.

4.2.1.3. Synthesis of single crystals and layers of $Ni_3B_7O_{13}Cl$ by transport of a preformed charge in a temperature gradient. In the case of the original three-crucible method the system is strongly off equilibrium during the growth of boracite owing to the presence of the starting material NiO in the ampoule. In that case the reaction can take place isothermally [19].

In an attempt at creating quasi-equilibrium conditions during the deposition of the layers and to regulate the deposition rate by changes of the three parameters: (i) mean temperature, (ii) temperature gradient, and (iii) quantity of the initial transport agent H_2O, attempts were made to transport a charge of $Ni_3B_7O_{13}Cl$, in contrast to the original method [19] where only some of the components need to migrate through the vapour phase.

In a first stage it was possible to demonstrate the transportability of $Ni_3B_7O_{13}Cl$ in a temperature gradient by keeping an excess of liquid B_2O_3 and solid $NiCl_2$ in the ampoule. In this way good and fairly large single crystals have been obtained (cf. table 5e) in a way analogous to the transport of Cr–Cl boracite (cf. table 5b).

In a second stage $Ni_3B_7O_3Cl$ layers have been produced on $Cr_3B_7O_{13}Cl$ under identical conditions. The properties of these layers were similar to those described in section 4.2.1.2.

4.2.1.4. Synthesis of $Ni_3B_7O_{13}Cl$ from the starting materials $B_2O_3(l)$, $NiCl_2(s)$ and $H_3BO_3(s)$. During the different variations of the synthesis of boracite with the ampoule method it has been found out – for Ni–Cl boracite and other boracite compositions as well – that boracite single crystals and layers can also be produced in the ampoule when the source material NiO, or $Ni_3B_7O_{13}Cl$, is entirely absent. In that case the NiO necessary for boracite formation is generated by hydrolysis of $NiCl_2$ by means of the water contained in the added H_3BO_3. The reaction proceeds until practically all the original H_2O of H_3BO_3 has

been consumed by the formation of hydrogen halide on the one hand and boracite on the other hand. Weighing of the boracite crystals formed in this way showed that the reaction proceeds nearly quantitatively. This result is in excellent accord with preliminary computer based calculations (cf. mode 6) showing that in the equilibrium state the vapour pressure of HCl exceeds by two orders of magnitude the next frequent species of the vapour phase, namely H_2O! These facts lead to the following conclusions:

(i) Independently of the particular method used (NiO source, Ni–Cl boracite source, absence of a NiO or Ni–Cl boracite reservoir) the initial stages of crystallization will proceed under continuously changing supersaturation of the various gas species until equilibrium is attained. This will be the case when practically the whole initially available H_2O quantity will be transformed to HCl and boracite.

(ii) It follows from point (i) that a reservoir containing NiO or Ni–Cl boracite is superfluous if thin layers are to be produced, because in that case the supersaturations will not appreciably change.

4.2.2. Chemical vapour deposition (CVD)

4.2.2.1. CVD apparatus and operation. The reactions tentatively postulated for the transport of preformed Ni–Cl boracite (cf. table 4, reaction numbers 1–4) can in principle also be used for the open-tube CVD synthesis of boracite if operated from right to left (table 4). An apparatus was therefore constructed (fig. 3), allowing the introduction, generation and mixing of the following reactants: $NiCl_2(g)$, $BCl_3(g)$, $H_2O(g)$, HCl(g), $H_3BO_3(g)$, $(HBO_2)_3(g)$, $HBO_2(g)$ and $(BOCl)_3(g)$.

The reaction chamber is a quartz tube placed in a tubular resistance heated furnace (fig. 3). The gaseous reactants are produced in the reaction zone behind the nozzle by one of the following two methods:

(i) The gaseous B_2O_3 hydrates and $(BOCl)_3$ are generated by passing H_2O vapour and HCl gas over a quartz boat containing liquid B_2O_3 (reactions 5 to 8). The substrate is placed above or right after the boat.

(ii) The gaseous B_2O_3 hydrates and $(BOCl)_3$ are generated by hydrolysing BCl_3 gas (reactions 16 to 19, table 3) in a HCl/H_2O stream. The substrate is placed

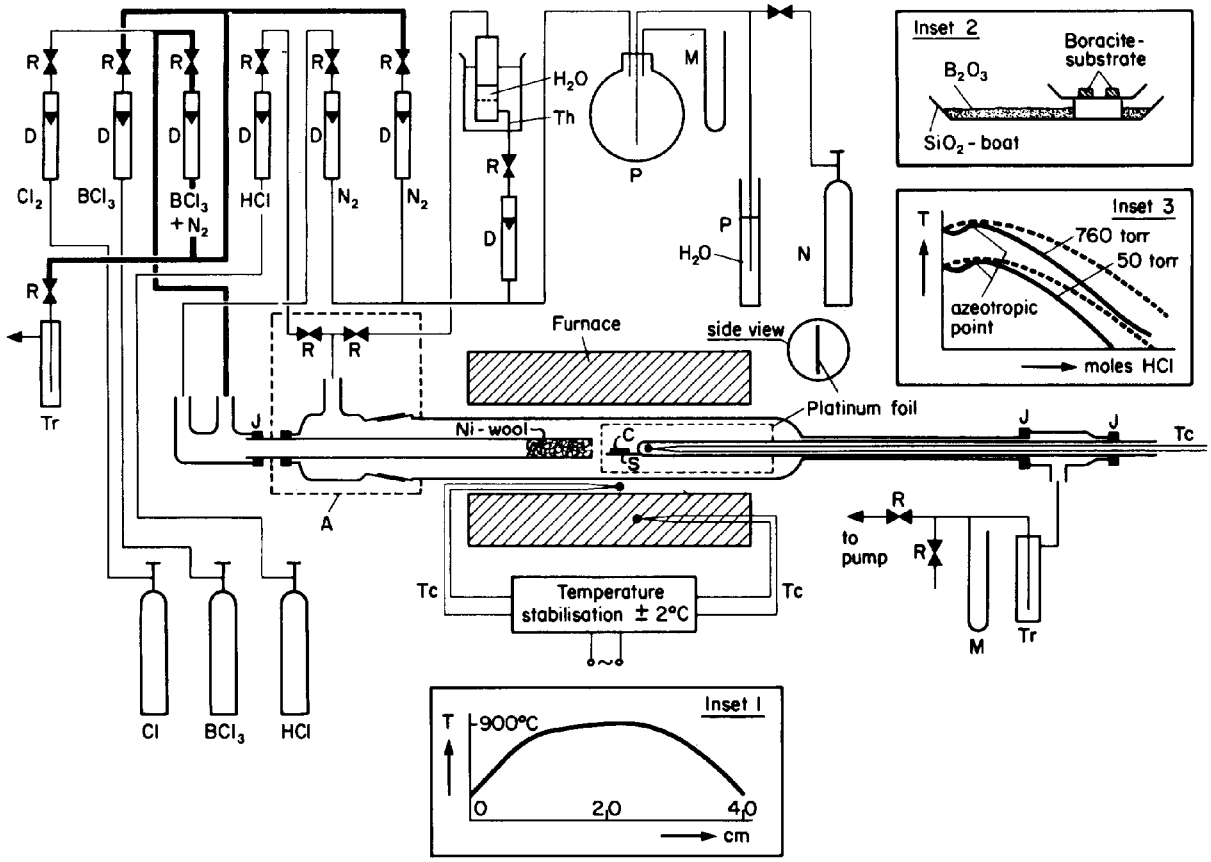

Fig. 3. CVD-apparatus for the deposition of $Ni_3B_7O_{13}Cl$.

close behind the nozzle letting in a mixture of $NiCl_2$ and BCl_3 gas.

For reasons of convenience the total pressure inside the reactor was kept equal to atmospheric pressure (or somewhat lower) for all experiments.

Remarks concerning the reactants

$NiCl_2$(g) vapour has been generated by passing chlorine at ~1000°C through a plug of nickel-wool placed in the inner tube (fig. 3). At that temperature and at the flow rates used (cf. table 4), the reaction $Ni + Cl_2 \rightarrow NiCl_2$ is practically quantitative. Thus the flow of Cl_2 may be equated to that of $NiCl_2$(g). In order to avoid condensation of solid $NiCl_2$, the partial pressure of $NiCl_2$ was always kept well below the saturation pressure, i.e. the flow rate of Cl_2 was always chosen in such a way that the partial pressure of $NiCl_2$ was ~20 Torr at 900°C.

H_2O(g): In both kinds of experiment (a and b) of the process H_2O(g) is led into the reactor by means of N_2 carrier gas bubbled through water of room temperature (fig. 3). The flowmeter measuring the rate of N_2 is placed before the entrance to the bubbler.

HCl(g) is taken from a cylinder and after having passed through a flowmeter, the HCl stream is admixed (valve R) to the N_2/H_2O stream. Hereafter the mixed gases enter the reaction zone via the outer tube, surrounding the inner, $NiCl_2$ generating tube.

Note: When HCl gas of room temperature is admixed to the N_2 stream having been saturated with H_2O vapour at room temperature, a H_2O/HCl condensate forms inside the mixing valve and its vicinity. This effect occurs because of the azeotropic nature of the liquid–vapour phase diagram of the HCl/H_2O system [27]. The system is schematically shown on inset 3 of fig. 3 for 50 and 750 Torr. As can be seen from the phase diagram, this condensation problem can be easily solved by placing an auxiliary heater (A) over the zone in question (fig. 3).

BCl_3(g): The development of the BCl_3 variant (b) of the CVD process was motivated by the results of Deiss and Blum [28] who unexpectedly obtained Mg–Cl, Fe–Cl and Cr–Cl boracite by passing a BCl_3/H_2 mixture over the corresponding oxides. In the case of nickel they obtained, however, only boride and possibly borate.

For operation of the BCl_3 hydrolysis process, BCl_3 gas is taken from a bottle, passed through a flowmeter and admixed to the Cl_2 stream. However, in order to keep the partial pressures of the boron oxide hydrates below their saturation pressures above B_2O_3(l), reactions 5 to 8 leading to the condensation of a growth blocking layer of B_2O_3(l), very small flow rates of BCl_3, smaller than the range of available flowmeters, had to be controlled. This has been achieved by diluting the primary BCl_3 stream by means of a N_2 stream and by subsequent control of the diluted stream by a flowmeter (fig. 3).

B_2O_3(l): In the hypothetical reaction equilibria (table 3) and in the overall discussion in this paper the liquid boron oxide phase, B_2O_3(l), is considered as pure. This is in fact an over-simplification and it is necessary to point out the following deliberately neglected facts:

(i) Liquid B_2O_3 dissolves SiO_2 of the SiO_2 crucible (etc.) to a considerable extent, e.g. about 65 mole% SiO_2 dissolves in B_2O_3 at 900°C. Although the SiO_2–B_2O_3 phase diagram is known [29], the time necessary for attaining the equilibrium is not.

(ii) The various species of the gas phase will be more or less soluble in the liquid, glassy B_2O_3/SiO_2 phase. These solubilities as a function of temperature, pressure and the concentration of the co-solvents are not known.

(iii) From (ii) it follows that for a given quantity of transport agent (e.g. initial H_2O) the total and partial pressures in the ampoule will depend upon the amount of the liquid phase present. Moreover, owing to the consumption of B_2O_3 during some of the synthesis modes (cf. table 6), these pressures will vary with time.

(iv) Probably there exist also silicon hydroxides (e.g. $Si_2O(OH)_6$, $SiO(OH)_2$ [30,31], and hydroxychlorides in the gas phase as well as in dissolved form in the B_2O_3/SiO_2 phase. Although the silicon compounds do not seem to participate in the boracite synthesis, they may influence the solubilities of their co-solutes in the B_2O_3/SiO_2 phase, some partial pressures and the total pressures.

The enumerated problems (certainly a not exhaustive list) show that at the present state of knowledge only a semiempirical approach can lead to experimental success.

4.2.2.3. The mixing of the reactant gases. The mixing of the reactant gases in the CVD reactor caused some difficulties. Owing to density differences

Table 6
Survey over the different modes of operation of CVT and CVD of Ni–Cl boracite; I_c = chemical individuals, R_i = independent reactions, ϕ = number of phases, F = variance

Process	Mode No	Condensed phases					Transport or reaction equilibria involved [a] (numbers correspond to table 4)	Thermal conditions for reaction	Phase rule $I_c - R_i + 2 - \phi = F$
		$NiCl_2$(s) Source	NiO(s) Source	B_2O_3(l) Source	$Ni_3B_7O_{13}Cl$(s) Source	$Ni_3B_7O_{13}Cl$(s) Product			
CVT	1	+	+	+		+	1–10	Isothermal or temp. gradient	11 – 7 + 2 – 5 = 1
	2		+	+		+	1–8, 10	Isothermal or temp. gradient	10 – 6 + 2 – 4 = 2
	3	+		+	+	+	1–9	Temp. gradient	10 – 6 + 2 – 4 = 2
	4			+	+	+	1–8	Temp. gradeint	9 – 5 + 2 – 3 = 3
	5	+		+		+	Idem mode 3	Isothermal or temp. gradient	10 – 6 + 2 –4 = 2
	6			+		+	Idem mode 4	Isothermal or temp. gradeint	9 – 5 + 2 – 3 = 3
CVD	1			+		+	1–8		9 – 5 + 2 – 3 = 3; 10 – 5 + 2 – 3 = 4 in presence of carrier gas
	2					+	1–4		8 – 4 + 2 – 2 = 4; 9 – 4 + 2 – 2 = 5 in presence of carrier gas

[a] Many more gas phase equilibria can be imagined; this fact does, however, not change the number of the degrees of freedom.

between the gases entering through the inner and those entering through the outer tube (fig. 3), the gases separated into layers and advanced by laminar flow. This has been monitored by means of a long rectangular platinum foil which has been placed vertically into the reactor tube right behind the nozzle (see fig. 3) and which worked as a "photographic plate". It showed the deposition of boracite crystals ($(111)_{cub}$ parallel to sheet) in a zone about 6 mm high and 10 cm long. Above and below this zone, similar zones of $3\,NiO \cdot B_2O_3$ were observed. Both boracite and borate occurred below the centre of the tube only. There was nearly no deposition in the upper half. This method – first described by Stein [26] for CVD of garnet layers – proved invaluable for determining the optimal location of the substrate. Only after such a study it was possible to obtain boracite layers free of spurious borate.

In an attempt to improve the mixing of the gases, simulation experiments at room temperature have been performed by means of the reaction $NH_3(g) + HCl(g) \rightarrow NH_4Cl(s)$ which produces a NH_4Cl(s) fog in the reaction zone. These experiments showed that best mixing was obtained with a slit-like nozzle, which creates turbulence.

4.3.2. Classification of the CVT and CVD growth experiments for layers and single crystals of $Ni_3B_7O_{13}Cl$ by means of the phase rule

As has been shown in the preceding paragraphs, the synthesis of layers and single crystals of $Ni_3B_7O_{13}Cl$ (and other boracite compositions) can be realized in a variety of ways. These differ in particular by the kinds of condensed phases present, the reaction equilibria involved and by the number of degrees of freedom available. The phase rule has been used in the form

$$I_c - R_i + 2 - \phi = F\,,$$

where I_c = number of chemical species, R_i = number of independent reactions, ϕ = number of phases and F =

degrees of freedom. This approach allows to understand reasonably well, on the basis of hypothetical reactions (see table 4), the various experimental situations encountered, and for example, the effects of a changing supersaturation on the quality of the crystals (cf. CVT mode 2).

In the philosophy of a more modern approach [39] the elements are considered as the components of the system and the auxiliary concept of "hypothetical reactions" can be dropped:

$$(\mathrm{Ni} + \mathrm{B} + \mathrm{O} + \mathrm{Cl} + \mathrm{H} = 5) + 2 - \phi = F\,.$$

This approach is of more general utility for the quantitative treatment, but because the chemical system is considered as a "black box" it may spring less to the eye at first sight.

The various situations are collected in table 6 and will be commented upon in the following section.

4.2.3.1. CVT in closed ampoules

CVT mode 1: This is the situation encountered in the three-crucible method [19] in which the reactants NiO, $NiCl_2$ and B_2O_3 are provided in three separately arranged crucibles, and where H_2O in the form e.g. of H_3BO_3 is introduced as the initial transport agent. The quantities of the reactants are chosen in such a way that during the conversion period of NiO to boracite, a surplus of solid $NiCl_2$ and liquid B_2O_3 is maintained. During that period there is only one degree of freedom, e.g. temperature. In practice this means that the system is off equilibrium until the last rest of NiO is consumed. This period is, however, characterized by a stationary kind of dynamic equilibrium which comes to an end with the disappearance of the last traces of NiO. At that point the system gains one more degree of freedom.

CVT mode 2 is identical with mode 1 except for the vapour pressure of $NiCl_2$ which lies below its saturation pressure, i.e. there is no condensed phase of $NiCl_2$ present. Because $NiCl_2$ is consumed during the boracite synthesis, the $NiCl_2$ pressure will decrease continuously. This means *monotonic* change of supersaturation with time and may lead to slight changes of the physical and chemical properties of the crystallized boracite (formation of growth layers [2]). In the case of iodine boracites the difficulty arises that owing to a high equilibrium pressure of iodine of the transition metal iodides very high iodine pressures would have to be maintained in the ampoule, in order to compel the system into mode 1 (double ampoule or autoclave necessary). Therefore, the so far grown Ni–I boracites [19] are carried out by mode 2.

CVT mode 3 describes the situation of transport of preformed Cr–Cl boracite (see section 4.1., step II) and Ni–Cl boracite (see section 4.2.1.3) where only the metal halide, B_2O_3(l) and boracite are present as condensed phases.

CVT mode 4 occurs if one attempts to transport Ni–Cl boracite in a temperature gradient with a pressure of $NiCl_2$ below its saturation pressure and a reservoir of B_2O_3(l) so as to avoid partial decomposition of the boracite during the transport.

CVT mode 5: This saturation occurs when only $NiCl_2$(s) and B_2O_3(l), together with some H_3BO_3 are introduced into the ampoule in such quantities that $NiCl_2$(s) and B_2O_3(l) are present at the reaction temperature. Then practically all the H_2O contained initially in H_3BO_3 is transformed to boracite on the one hand and to HCl on the other.

CVT mode 6 is exemplified when one starts with B_2O_3(l) and some unsaturated vapour of $NiCl_2$ in the ampoule. Then the H_2O of the initial H_3BO_3 may be transformed to boracite as in mode 5.

4.3.1.1. CVD

CVD mode 1 corresponds to the situation where the gaseous boron oxide hydrates and $(BOCl)_3$ are obtained by reaction of H_2O/HCl gas with B_2O_3(l) (reactions 5 to 8). In the presence of a carrier gas, the number of degrees of freedom is four (for example: total pressure, temperature, H_2O/HCl pressure ratio, and $NiCl_2$ partial pressure).

CVD mode 2 applies if the gaseous boron oxide hydrates and $(BOCl)_3$ are produced by means of hydrolysis of BCl_3 in such a way as to avoid the condensation of B_2O_3(l) (see section 4.2.2.2). As can be seen from table 6 the CVD mode 2 offers the largest number of degrees of freedom (five, if a carrier gas is used). Therefore it is the most versatile but also the most difficult experimental situation because all these parameters have to be rigorously controlled.

5. Properties of the $Ni_3B_7O_{13}Cl$ layers

5.1. CVT layers

The quality of the CVT layers was very much superior to those obtained by CVD. The properties

of the CVT layers will therefore be discussed in some detail in this paragraph.

5.1.1. Nucleation of the layers

In an attempt to obtain a glimpse of the initial stages of growth, a Cr–Cl boracite substrate with growth steps (step height 0.1 μm) and very smooth intermediate terraces (fig. 4a) has been inserted during 5 min into the furnace. This resulted in a maximal temperature of 825°C inside the ampoule (test on dummy). As can be seen from the photograph in reflected light and Nomarski contrast, small islands of about 550 Å thickness have been formed on the terraces (fig. 4b). Along the steps the islands have already collapsed, showing easier nucleation along these lines. The domains were too thin for the determination of the orientation of the spontaneous polarization by optical means.

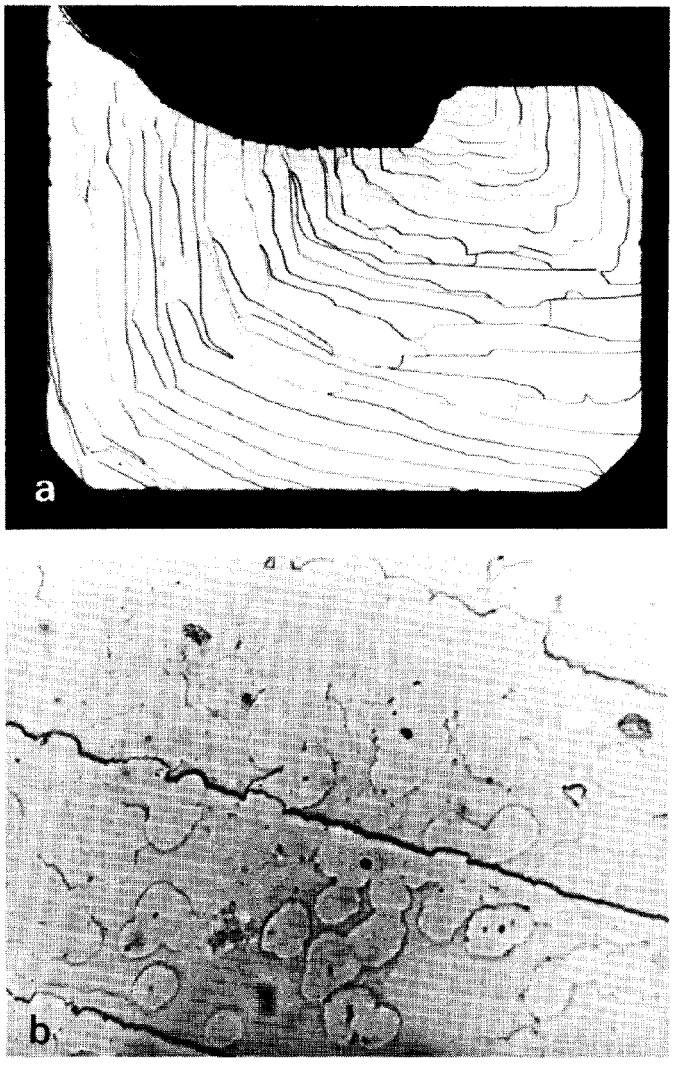

Fig. 4. Nucleation stage of Ni–Cl boracite on a Cr–Cl boracite substrate; (a) as-grown substrate; (b) initial islands of layer (thickness ~550 Å).

5.1.2. The thickness of the produced layers

The thickness of the produced layers ranged between <1 and 100 μm. The measurement of the thickness was done by one or both of the following two methods:

(i) If the ferroelectric domains of Ni–Cl boracite are oriented with their spontaneous polarization perpendicular to the surface, the birefringence $\Delta n_{\gamma,\alpha} = 0.022$ [2] corresponds to that orientation. By measuring the retardation by means of a compensator, the thickness d is obtained by the relation $d = \Gamma/\Delta n_{\gamma,\alpha}$, where Γ is the path difference. The method is not applicable if spurious domains of other orientations interfere.

(ii) By preparing a polished orthogonal section through the sandwich substrate + layer, the layer thickness can be measured directly by means of a measuring ocular.

Both methods have an accuracy of about ±0.8 μm for an objective 40X and an ocular 20X.

5.1.3. The smoothness or roughness of the layer surface

The smoothness or roughness of the layer surface is essentially ruled by the quality of the substrate surface. The smoothest layer surface was obtained on substrates on which no growth centre and no growth step could be seen (fig. 5). The next best layers were those obtained on as-grown substrates with a single growth centre and flat vicinal facets showing no growth steps (fig. 6a). By means of Nomarski interference contrast (fig. 6b) many tiny growth hillocks indicate a very homogeneous distribution of nuclei. The very homogeneous extinction in transmission (fig. 6c) indicates a very uniform thickness (about 1 μm).

Polished surfaces (fig. 7a) often resulted in layers with uneven growth hillocks (figs. 7b and 7c).

5.1.4. Domain properties

5.1.4.1. Static properties. The as-grown CVT layers of a thickness equal or smaller than about 10 μm were characterized by ferroelectric domains with the

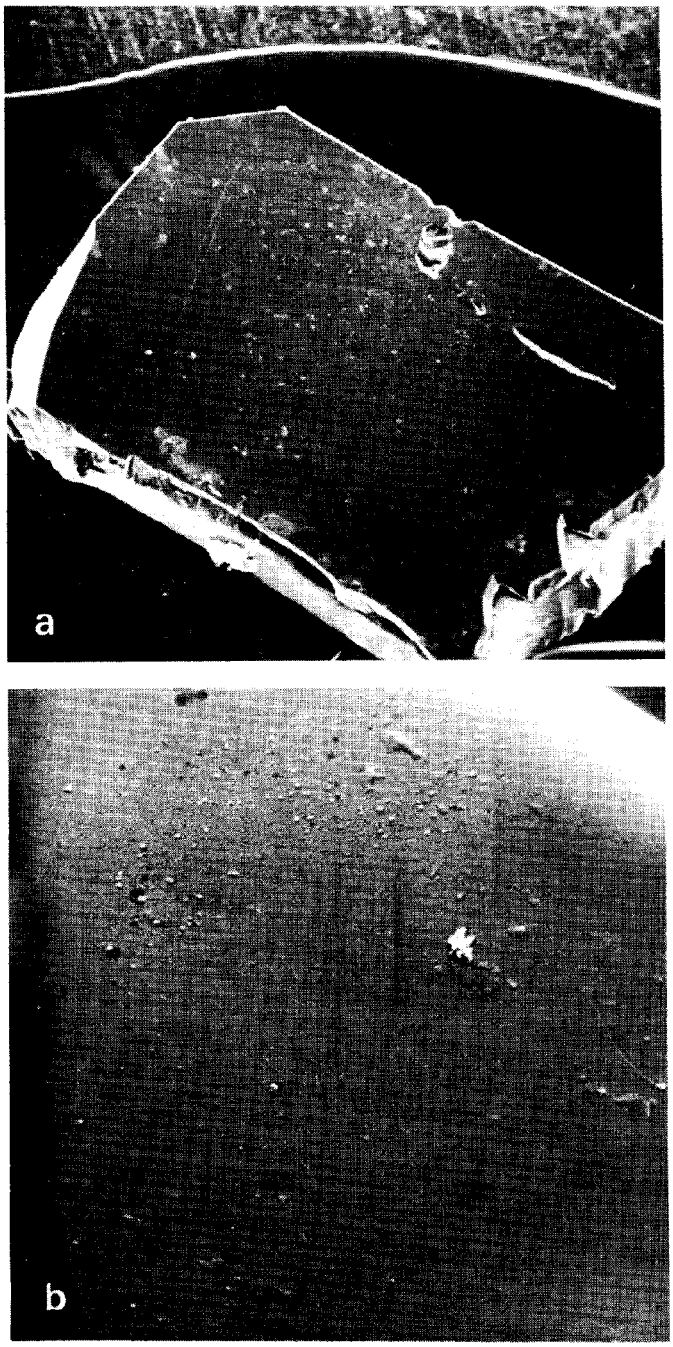

Fig. 5. Scanning electron microscope view of a very smooth surface of a Ni–Cl boracite layer 102 μm thick; (a) 75X; (b) 3750 X.

spontaneous polarization oriented up and down (fig. 8) only. With a magnification of 800X, domains with a diameter below 1 μm can be seen. The domain walls appear as dark lines, if viewed with crossed polarizers (fig. 8a), with an apparent width of about 0.3 μm.

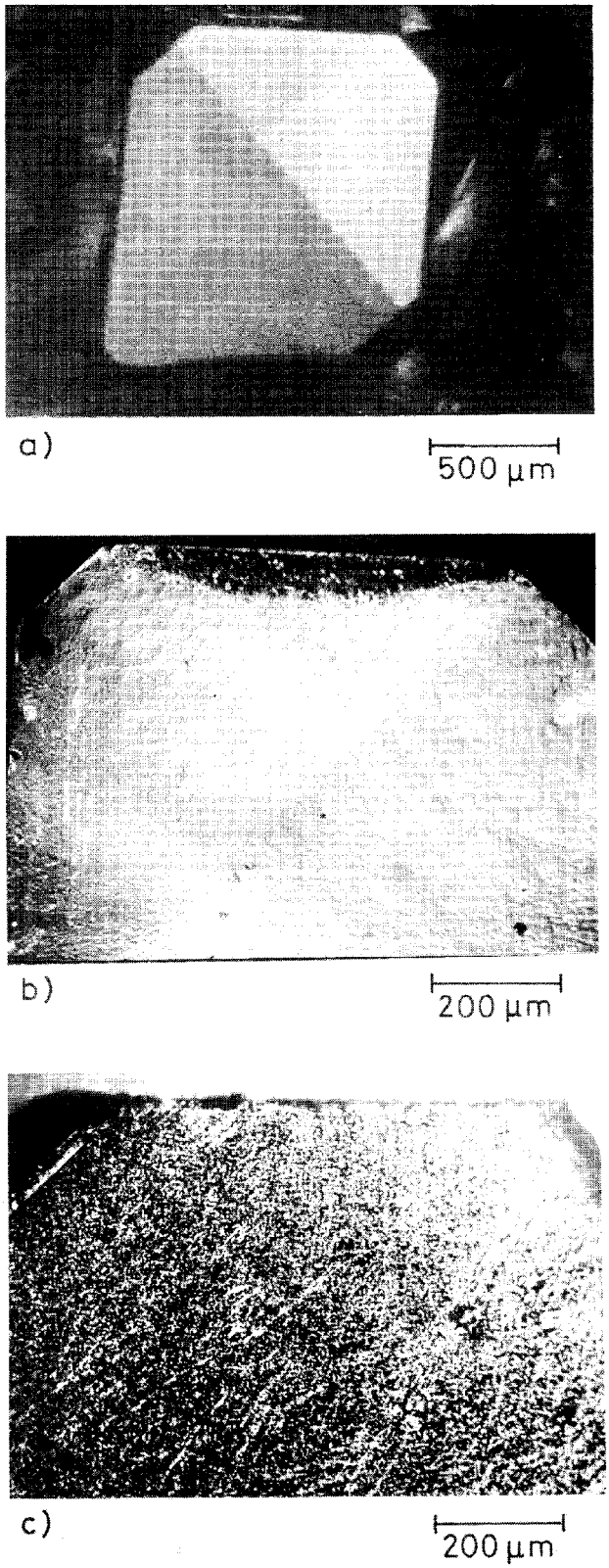

Fig. 6. Layer of Ni–Cl boracite (1 μm thick) on Cr–Cl boracite (70 μm thick) prepared in a sealed ampoule. Up-down domains only. (a) Virgin surface of substrate, one growth centre, vicinal facets without visible growth steps. (b) Surface of layer in reflected light, Nomarski contrast. (c) Layer in transmitted light, crossed polarizers, path difference compensated for one domain orientation.

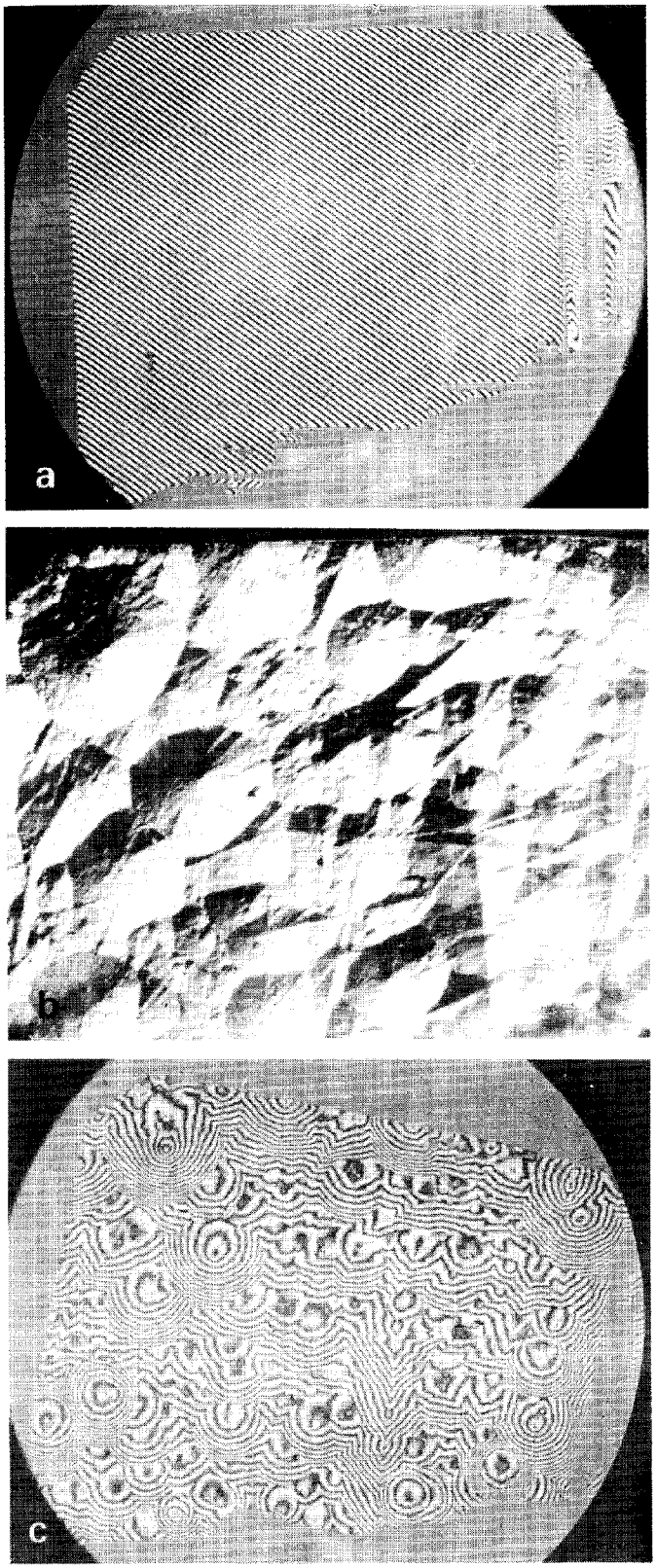

Fig. 7. Growth of a Ni–Cl boracite layer on a polished substrate; (a) polished substrate, interference fringes; (b) growth hillocks on layer, Nomarski contrast; (c) interference fringes corresponding to (b).

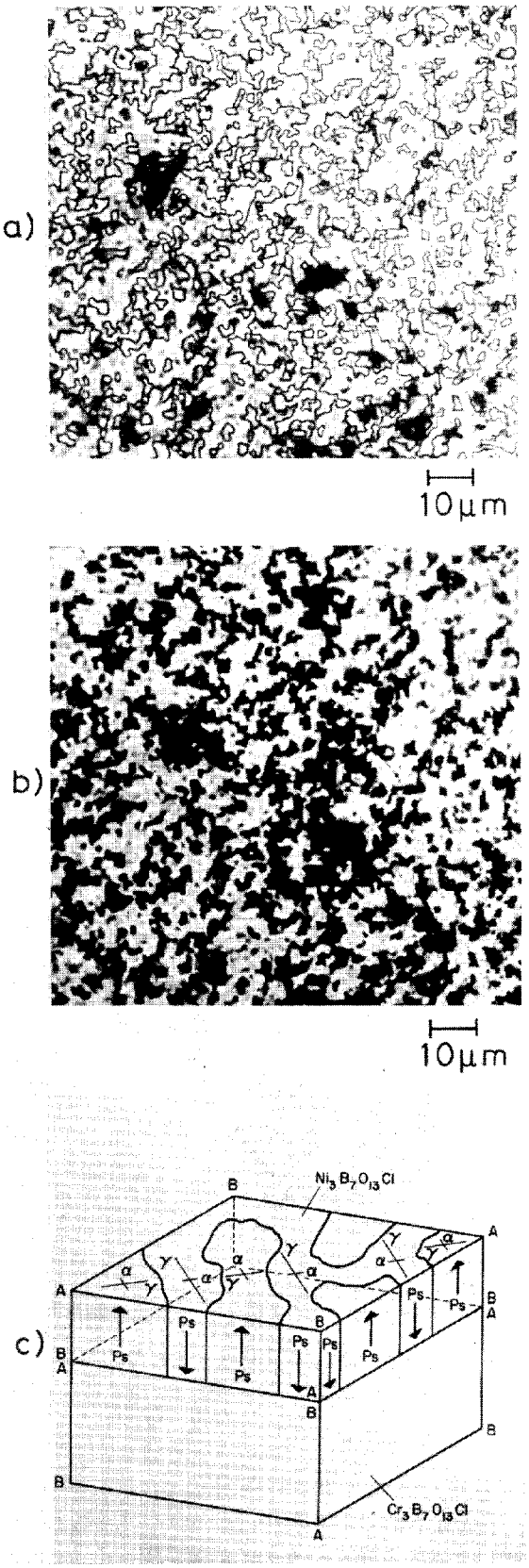

Fig. 8. Ferroelectric domains with antiparallel spontaneous polarization (perpendicular to surface) of a 2 μm thick layer of Ni–Cl boracite on Cr–Cl boracite (70 μm thick); ampoule CVT method; filter: λ = 546 nm; transmitted light: (a) crossed polarizers, vibration direction parallel $\langle 100\rangle_{cub}$; (b) ditto, but compensation of path difference for domains of one of the polarities; (c) schematic.

However, since the resolving power $\lambda/2A$ was 0.32 μm (wavelength $\lambda = 0.55$ μm, aperture $A = 0.85$) the real thickness is probably much smaller.

The two kinds of thickness measurement (see section 5.1.2) gave the same result showing that the domains penetrated the entire thickness of the layer.

Layers with a thickness above about 10 μm usually showed also domains having their spontaneous polarization oriented within the plane of the layer. This shows that for thin layers there exists a mechanical interaction with the substrate, whereas thick layers behave like free bulk crystals.

In some samples the regions (domains) with equal orientation of polarization were much larger (fig. 9). In that case fine lines were observed which were surrounded on either side by domains of equal orientation of polarization. These lines are supposed to be micro-fissures.

5.1.4.2. Quasistatic switching. The testing of the switching of the samples was done in three different ways:

(i) Sample without electrodes, transparent In_2O_3

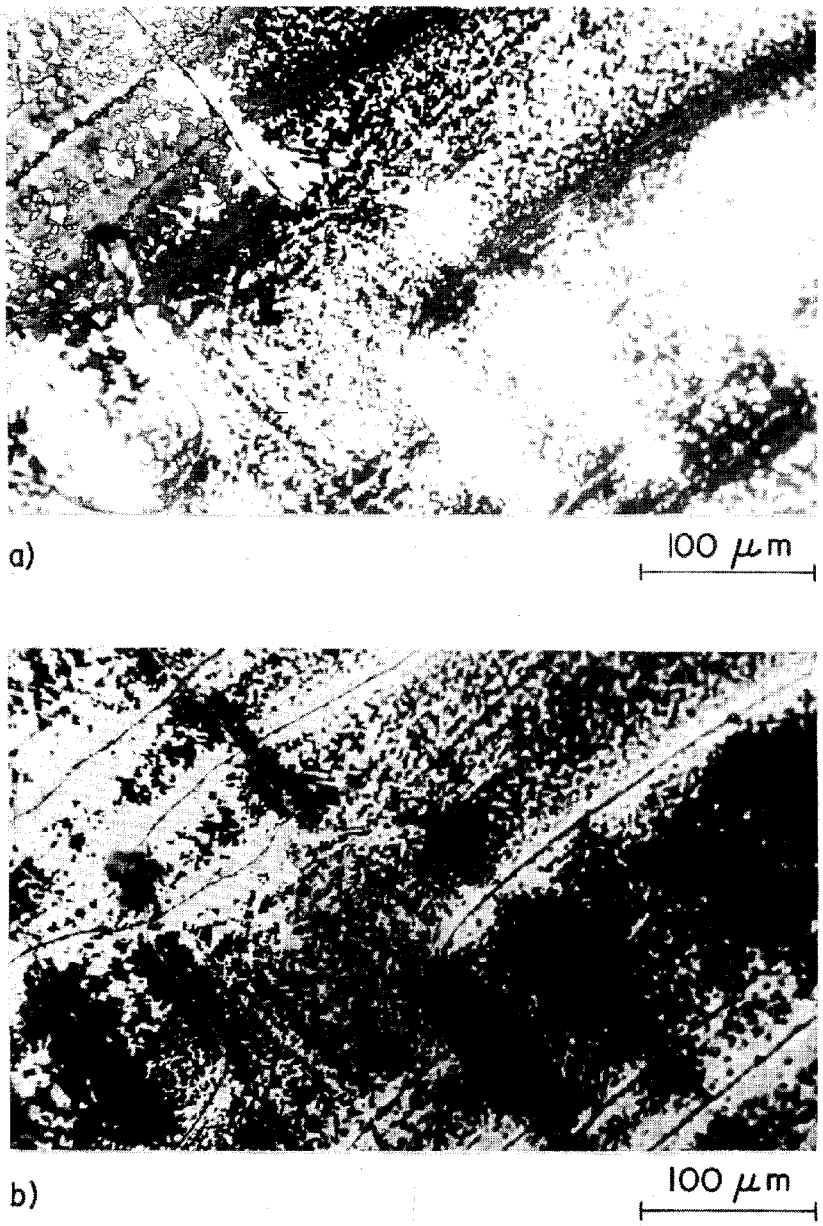

Fig. 9. Large ferroelectric up-down domains of a Ni–Cl boracite layer (thickness 5–6 μm). (a) and (b) correspond to compensation of the path difference of the opposite domains; the net of lines is probably caused by microfissures.

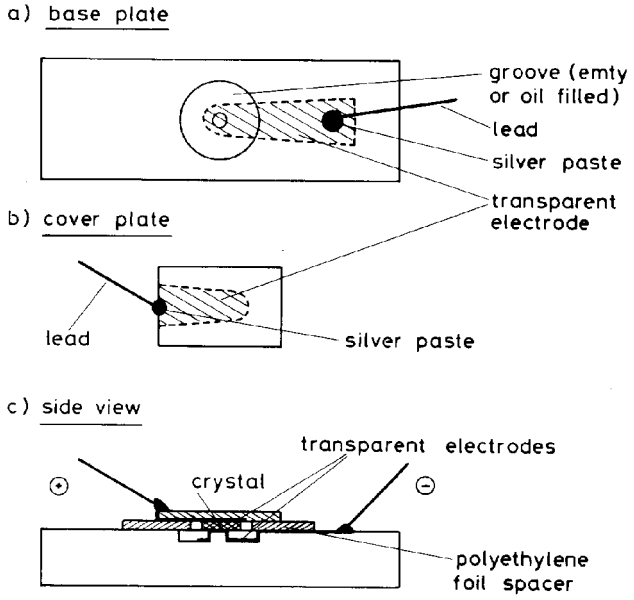

Fig. 10. Switching device for ferroelectric plate-like samples with or without electrodes.

electrodes of switching device (fig. 10) in direct contact with sample.
(ii) Test as under (i) but layer covered with transparent In_2O_3 electrode.
(iii) Test as under (i) but after removal of In_2O_3 layer of (ii) by means of HCl.

For a particular sample (fig. 11) the poling of the ferroelectric layer started at about 100 kV cm^{-1} and saturation was achieved at ~500 kV cm^{-1} for one polarity (fig. 11c), with nearly 100% remanence (fig. 11d). For the opposite polarity only about one third of the surface was saturable (fig. 11a) and the remanence of that part was less than 100% (fig. 11b). The same sample under condition (ii) could not be switched at all, whereas after removal of the In_2O_3 electrode, the initial behaviour has been reestablished. This showed that the In_2O_3 electrode blocked the switching entirely by mechanical interaction (blocked ferroelasticity). The substrate–layer interaction seems to block only partially.

5.2. *Properties of CVD layers*

The quality of the layers achieved with the CVD experiments was much less satisfactory than that

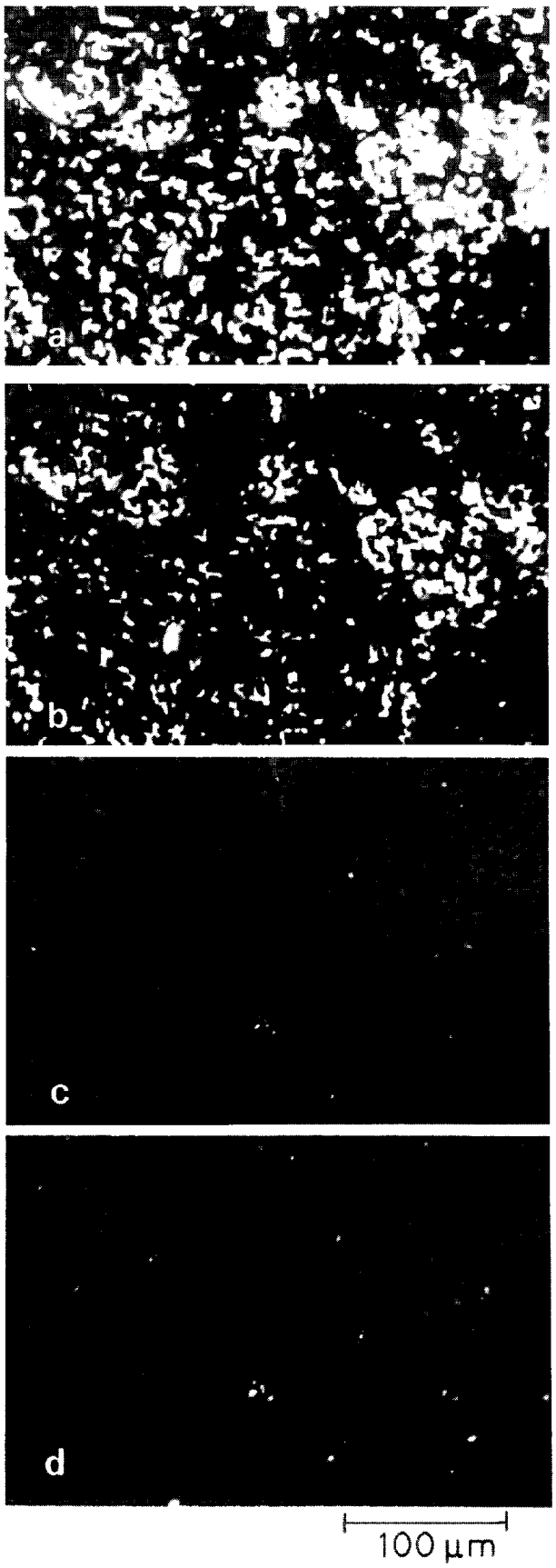

Fig. 11. Switching properties of a 2 µm thick layer of Ni–Cl boracite on a 50 µm thick substrate of Cr–Cl boracite; transparent gold electrodes; (a) +500 kV cm^{-1}; (b) remanence of (a); (c) −500 kv cm^{-1}; (d) remanence of (c).

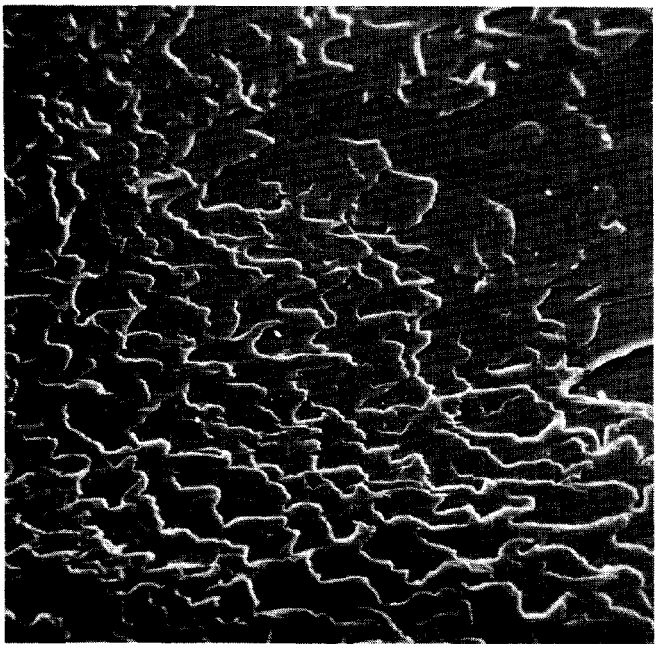

Fig. 12. Scanning electron microscope photograph (385X) of the surface of a Ni–Cl boracite layer grown by the BCl_3–CVD process (385X).

obtained by the CVT process. A typical surface state is shown in fig. 12 (scanning electron microscope photograph) which shows a strong influence of the gas flow. The layers did not show the up-down patterns. The switching behaviour has not been studied.

6. Some thermodynamic considerations

In table 4 some plausible reactions have been written down concerning CVT and CVD of $Ni_3B_7O_{13}Cl$, B_2O_3, $NiCl_2$, $(3\,NiO)\cdot B_2O_3$ and NiO (reactions 1 to 14). The convention used by Schäfer [32] for transport reactions of writing the condensed phase on the left hand side of the equation, has been respected. If the equations are read from right to left, they describe CVD synthesis reactions. The reaction enthalpy $(\Delta H^\circ_{298})^R$, the reaction entropy $(\Delta S^\circ_{298})^R$, the free energy of reaction at 1147 K, $(\Delta G^\circ_{1147})^R$ and the logarithm of the equilibrium constant K_p have also been indicated in table 4.

The free energy of reaction and the equilibrium constant have been calculated by means of the so-called "First Approximation":

$$(\Delta H^\circ_{298})^R - T(\Delta S^\circ_{298})^R = (\Delta G^\circ_T)^R$$
$$= -RT\,2.303\log K_p\,.$$

Table 7
Some data of enthalpy and entropy of formation, used in the calculation of the approximated equilibrium constants, given in table 4

Compound	ΔH°_{298} (kcal mol^{-1})	S°_{298} (cal deg^{-1} mol^{-1})	Ref.
HCl(g)	−22.063 ± 0.05	44.645	[41]
H_2O(g)	−57.7979	45.106	[41]
$NiCl_2$(g)	−14.3	73.2	[40]
NiO(s)	−58.4	9.22	[40]
$(3NiO)B_2O_3$(s)	[⩽ −482] a)	[40.6] b)	Estimated this paper
$Ni_3B_7O_{13}Cl$(s)	[⩽ −1249] a)	[81.2] b)	Estimated this paper
B_2O_3(l)	−299.28 ± 0.4	18.739	[41]
H_3BO_3(g)	−237.16 ± 0.6	[70.539] b)	[41]
HBO_2(g)	−134.0 ± 1	[57.273] b)	[41]
$(HBO_2)_3$(g)	−543 ± 3	[83.047] b)	[41]
$(BOCl)_3$(g)	−390 ± 2	[91.367] b)	[41]
BCl_3(g)	−96.31 ± 0.5	69.328	[41]

a) ΔH°_{298}, reaction from $3NiO + B_2O_3$, and $\frac{5}{2}NiO + \frac{7}{2}B_2O_3 + NiCl_2$, increased negatively by 1%, real value probably still more negative.

b) S°_{298}: by using "Kelley's sum rule", see e.g. ref. [38]. this paper.

The positive sign of $(\Delta H^\circ_{298})^R$ of the CVT reactions of $Ni_3B_7O_{13}Cl$ reactions 1 to 4), $(3\,NiO)\cdot B_2O_3$ (reactions 11 to 14), NiO (reaction 10) and B_2O_3 (reactions 5 and 8) indicates [32] that transport should occur from the higher to the lower temperature. This expectation has repeatedly been confirmed for $Ni_3B_7O_{13}Cl$ (see section 4). The negative sign of $(\Delta H^\circ_{298})^R$ of reactions 6 and 7 shows their tendency to transport B_2O_3 also in the opposite sense.

The negative sign of $\log K_p$ shows that all the equilibria listed are shifted to the left hand side. However, the relatively small absolute value of $\log K_p$ of reactions 3 and 6 would suggest that the boracite and B_2O_3 transport essentially proceeds via $(HBO_2)_3$. Because $\log K_p$ of reactions 5, 7, 8, 17 and 19 is rather small, too, the participation of HBO_2, H_3BO_3, $(BOCl)_3$, BCl_3 cannot be excluded. At this stage no statement can be made concerning the reaction mechanisms at the surface of the crystals.

As can be seen from fig. 13, the partial pressure of HBO_2 dominates below about 120 Torr (at 874°C) H_2O pressure and the pressures of H_3BO_3 and $(HBO_2)_3$ dominate above about 120 Torr H_2O if

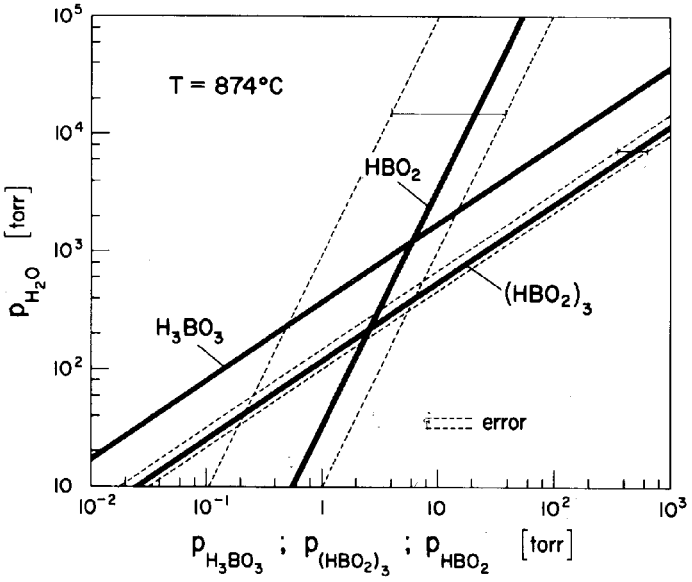

Fig. 13. Equilibrium vapour pressure of H_2O versus equilibrium partial pressures of the B_2O_3 hydrates (data used from ref. [33]).

liquid B_2O_3 is present. The boracite syntheses were all carried out below 10^2 Torr H_2O where HBO_2 is the dominating boron/oxide hydrate. The curves of fig. 13 have been calculated using the K_p data of Blauer and Farber [33] for reactions 5, 6 and 7. Because no error limits had been given for the experimentally determined K_p of reaction 7, the curve corresponding to H_3BO_3 may in reality be shifted parallel to itself to an appreciable extent.

With a view to the great number of gaseous species present in the CVD and CVT synthesis of boracites, future studies of the chemistry of boracite synthesis will require computer based equilibrium (etc.) calculations using a free energy minimization approach. In a preliminary trial Diehl [34] has calculated the partial pressures of the gaseous species for the case of CVT of $Ni_3B_7O_{13}Cl$ using the approach and program of Noläng and Richardson [35–37]. The results are shown in table 8.

The interesting features of Diehl's computation are the following:

(i) the only condensed phases occurring are $Ni_3B_7O_{13}Cl$ and B_2O_3(l). This means that partial decomposition of boracite occurs under the chosen conditions. As has been shown by experiment (see section 4.2.1.3), the decomposition of Ni–Cl boracite to B_2O_3 is entirely suppressed if B_2O_3(l) and $NiCl_2$(s) are charged into the ampoule right from the beginning.

(ii) The total pressure is nearly entirely made up of HCl gas, a result which agrees well with experiment (see section 4.2.1.4),

(iii) Beside the intially proposed gaseous species (see table 4) it is interesting to note that also H_2, Cl_2, Cl, NiCl and BOCl have to be considered, if about 10^{-4} atm is taken as a lower limit of importance for the partial pressure.

(iv) The case where the total pressure equals 1 atm (table 8), comes close to the conditions for CVD which was nearly always run at about 1 atm total pressure (see section 4.2.2). The case where the total pressure equals 5 atm comes close to the CVT conditions realized in the closed ampoules [19] and which were sometimes run even up to a total pressure of about 15 atm.

(v) Table 8 shows well how the relative importance of $(BOCl)_3$, BCl_3, H_3BO_3 and $(HBO_2)_3$ increases as expected in passing from a total pressure of 1 to 5 atm.

More detailed work on the thermodynamic basis of boracite synthesis is underway.

Table 8
Calculated activities (partial pressures) for the CVT of Ni–Cl boracite (according to Diehl [34]); arbitrarily chosen parameters: temperature: 900°C; initial mole numbers: 10 mole $Ni_3B_7O_{13}Cl$ and 1 mole HCl

Vapour species	Total pressure 1 atm	Total pressure 5 atm
	Partial pressure (atm)	Partial pressure (atm)
HCl	0.983	$0.493 \times 10^{+1}$
$NiCl_2$	0.920×10^{-2}	0.396×10^{-1}
H_2O	0.769×10^{-2}	0.335×10^{-1}
$(BOCl)_3$	0.240×10^{-4}	0.331×10^{-3}
HBO_2	0.490×10^{-4}	0.102×10^{-3}
H_2	0.311×10^{-4}	0.150×10^{-3}
BCl_3	0.166×10^{-4}	0.230×10^{-3}
Cl_2	0.264×10^{-4}	0.137×10^{-3}
Cl	0.186×10^{-4}	0.423×10^{-4}
H_3BO_3	0.101×10^{-4}	0.925×10^{-4}
NiCl	0.923×10^{-5}	0.174×10^{-4}
$(HBO_2)_3$	0.750×10^{-5}	0.683×10^{-4}
BOCl	0.515×10^{-6}	0.124×10^{-5}

7. Conclusions

The synthesis of epitaxial boracite layers by means of CVT and CVD has proved feasible. Sofar the best layers have been obtained by CVT. The CVD methods also appear promising for making single crystals and mixed crystals. Further improvement of the methods will require studies of thermodynamic parameters, phase diagrams, reaction kinetics, reaction mechanisms and gas dynamics (mixing). For the technical application (electro-optics) of the layers, the development of shear free compositions and conducting transparent substrates would be mandatory.

Acknowledgements

Grateful acknowledgements are extended to Thomson–CSF, France, and Montecatini–Edison S.p.A., Italy, who jointly sponsored this work (executed in 1971). Particular thanks go to Dr. G. Lanzavecchia (Montecatini–Edison) and Dr. G. Pircher (Thomson–CSF) for continued critical stimulation. Gratefulness is also extended to Dir. Dr. H. Thiemann and Dr. J.-C. Courvoisier of Battelle Geneva, whose efforts allowed the international character of the project to materialize. Thanks go also to Dr. J. Figar for help at the beginning of the project.

The authors are very grateful to Dr. R. Diehl, Institut für Angewandte Festkörperphysik, Freiburg i. Br., for some computer-based computations of partial pressures (1978) and for suggesting improvements of the manuscript. Special thanks are due also to Dr. M.W. Richardson, Uppsala University, for his critical reading of the manuscript which led to many improvements.

References

[1] K. Aizu, Phys. Rev. B2 (1970) 754.
[2] H. Schmid, Rost Kristallov 7 (1967) 32 (English Transl. Growth of Crystals 7 (1969) 25).
[3] L.A. Petermann and H. Schmid, Rev. Phys. Appl. 11 (1976) 449.
[4] H. Schmid and H. Tippmann, Ferroelectrics 20 (1978) 21.
[5] H. Schmid and J. Schwarzmüller, Ferroelectrics 10 (1976) 283.
[6] A. Kumada, IEEE Trans. ED-20 (1973) 866.
[7] J.R. Barkeley, L.M. Brixner, E.M. Hogan and R.K. Waring, Jr, Ferroelectrics 3 (1972) 191.
[8] T.A. Kravchuk and Yu.D. Lazebnik, Russ. J. Inorg. Chem. 12 (1967) 21.
[9] C. Fouassier, A. Levasseur, J.C. Joubert, J. Muller and P. Hagenmuller, Z. Anorg. Allgem. Chem. 375 (1970) 202.
[10] J. Joubert, J. Muller, C. Fouassier and A. Levasseur, Kristall und Technik 6 (1971) 65.
[11] A. Levasseur, C. Fouassier and P. Hagenmuller, Mater. Res. Bull 6 (1971) 15.
[12] W. Jeitschko and T.A. Bither, Z. Naturforsch. 27b (1972) 1423.
[13] J.C. Joubert, J. Muller, M. Pernet and B. Ferrand, Bull. Soc. Franc. Mineral. Crist. 95 (1972) 68.
[14] J. Muller, Sur la Stabilité de Quelques Phases Boracites en Milieu Hydrothermal, Thesis, Univ. of Grenoble (1970).
[15] A. Levasseur, Thesis (No. 409), Univ. of Bordeaux (1973).
[16] A. Levasseur, B. Rouby and C. Fouassier, Compt. Rend. (Paris) 277 (1973) 421.
[17] T.A. Bither and H.S. Young, J. Solid State Chem. 10 (1974) 302.
[18] T.A. Grigor'eva, Izv. Akad. Nauk SSSR, Neorgan. Mater. 12 (1976) 1691. (English Transl. Inorg. Mater. 12 (1977) 1392).
[19] H. Schmid, J. Phys. Chem. Solids 26 (1965) 973.
[20] V.I. Bugakov, N.N. Sheftal and T.I. Timchenko, Izv. Akad. Nauk SSSR, Neorgan. Mater. 8 (1972) 1947 (English Transl. Bull. Akad. Sci. USSR, Inorg. Mater. 8 (1973) 1713).
[21] V.I. Bugakov, V.P. Orlovski and N.N. Sheftal, Izv. Akad. Nauk SSSR, Neorgan. Mater. 9 (1973) 2141 (English Transl. Bull. Akad. Sci. USSR, Inorg. Mater. 9 (1974) 1890).
[22] K. Nassau and J.W. Shiever, J. Crystal Growth 16 (1972) 59.
[23] T. Takahashi and O. Yamada, J. Crystal Growth 33 (1976) 361.
[24] N.N. Nesterova, R.V. Pisarev and G.T. Andreeva, Phys. Status Solidi (b) 65 (1974) 103.
[25] R.V. Pisarev, V.V. Druzhinin, S.D. Prochorova, N.N. Nesterova and G.T. Andreeva, Phys. Status Solidi 34 (1969) 145.
[26] B.F. Stein, J. Appl. Phys. 42 (1971) 2336.
[27] Landolt–Börnstein's Tabellen, Vol. IIa (1960) pp. 171–172.
[28] W.J. Deiss and P. Blum, Compt. Rend. (Paris) 244 (1957) 464.
[29] R.J. Charles and F.E. Wagstaff, J. Am. Ceram. Soc. 51 (1968) 16.
[30] O. Glemser, Österr. Chemikerz. 64 (1963) 301.
[31] I. Barin and O. Knacke, Thermochemical Properties of Inorganic Substances (Springer, Berlin, 1973); supplement: I. Barin, O. Knacke and O. Kubaschewski, Thermochemical Properties of Inorganic Substances (Springer, Berlin, 1977).

[32] H. Schäfer, Chemische Transportreaktionen (Verlag Chemie, Weinheim, 1962) (English Transl. Chemical Transport Reactions (Academic Press, New York, 1964)).
[33] J.A. Blauer and M. Farber, J. Phys. Chem. 68 (1964) 2357.
[34] R. Diehl, Institut für Angewandte Festkörperphysik Freiburg i. Br., private communication.
[35] B.I. Noläng and M.W. Richardson, J. Crystal Growth 34 (1976) 198.
[36] B.I. Noläng and M.W. Richardson, J. Crystal Growth 34 (1976) 205.
[37] M.W. Richardson and B.I. Noläng, J. Crystal Growth 42 (1977) 90.
[38] W.S. Knapp and W.D. van Horst, J. Am. Ceram. Soc. 34 (1952) 384.
[39] W. Depmeier, H. Schmid, B.I. Noläng and M.W. Richardson, J. Crystal Growth 46 (1979) 718.
[40] Handbook of Chemistry and Physics (The Chemical Rubber Publishing Corp., Cleveland, Ohio, 1960).
[41] D.R. Stull and H. Prophet, JANAF, Thermochemical Tables, 2nd ed. (Natl. Bur. Std., 1971).
[42] F.D. Rossini et al., Selected values of chemical thermodynamic properties, Circular Natl. Bur. Std., No. 500 (1952).
[43] K.K. Kelley and E.G. King, Bull. Bur. Mines, No. 592 (1961).